Journal of Hazardous Materials 186 (2011) 1560–1567

Contents lists available at ScienceDirect

Journal of Hazardous Materials

journal homepage: www.elsevier.com/locate/jhazmat

Preparation, characterization and activity evaluation of TiN/F-TiO_2 photocatalyst

Chen Shifu*, Yang Yunguang, Liu Wei*

Department of Chemistry, Huaibei Normal University, Anhui, Huaibei, 235000, People's Republic of China

ARTICLE INFO

Article history:
Received 23 July 2010
Received in revised form 9 December 2010
Accepted 9 December 2010
Available online 17 December 2010

Keywords:
Photocatalyst
TiN/F-TiO_2
Preparation
Characterization
Activity
Ball milling

ABSTRACT

In this paper, F-TiO_2 and TiN/F-TiO_2 nanoparticle photocatalysts were prepared by ball milling. The photocatalysts were characterized by X-ray powder diffraction (XRD), scanning electron microscopy (SEM), transmission electron microscopy (TEM), terephthalic acid photoluminescence probing technique (TA-PL), X-ray photoelectron spectroscopy (XPS), and UV–vis diffuse reflection spectroscopy (DRS). The photocatalytic activity of the photocatalysts was evaluated by photocatalytic degradation of methylene blue (MB) and rhodamine B (RhB). The results showed that the photocatalytic activity of the F-TiO_2 was much higher than that of TiO_2, and the photocatalytic activity of the TiN/F-TiO_2 was much higher than that of TiO_2 and F-TiO_2 under UV light irradiation. The optimum percentage of doped TiN is 0.2 wt.%. Compared with pure TiO_2, the photoabsorption wavelength range of the TiN/F-TiO_2 and F-TiO_2 photocatalysts red shifts and improves the utilization of the total spectrum. The effect of ball milling time on the photocatalytic activity of the photocatalysts was also investigated. The optimum ball milling time is 12 h. The mechanisms of influence on the photocatalytic activity of the photocatalysts were also discussed.

1. Introduction

In recent years, the photocatalytic degradation of various kinds of organic and inorganic pollutants using semiconductor powders as photocatalysts has been extensively studied since Fujishima and Honda discovered the photocatalytic splitting of water on TiO_2 electrodes in 1972 [1,2,3]. Owing to its relatively high photocatalytic activity, biological and chemical stability, low cost, non-toxicity, and long-term stability against photocorrosion and chemical corrosion, TiO_2 has been widely used as a photocatalyst [4,5]. However, the photocatalytic activity of TiO_2 is limited to irradiation wavelengths in the UV region, thus the effective utilization of solar energy is limited to about 3–5% of the total solar spectrum. Some problems still remain to be solved, such as the fast recombination of photogenerated electron–hole pairs. Therefore, to improve the photocatalytic activity by modification has become a hot topic among researchers in the last decade [6,7]. Many investigators have quested for various methods, such as doping transition metals [8,9,10,11], doping non-metallic elements [12,13,14,15,16], and forming composite photocatalysts from different semiconductors [17,18,19,20], etc., to enhance the photocatalytic activity of TiO_2 and to improve the utilization of visible light. The results showed that nearly all the composite semiconductors had higher photocatalytic activity than single ones.

Recently, fluorinated TiO_2 (F-TiO_2) has been investigated extensively to enhance the photocatalytic activities. It was proposed that the fluorinated surface favored the generation of free OH radicals. Meanwhile, the photoabsorption wavelength of the photocatalyst was extended [21,22,23]. The composite photocatalyst TiN/TiO_2 has been studied in our earlier report and the photocatalytic activity is improved for doping appropriate Ti^{3+}, which can act as a reactive center on the surface [24]. When TiN integrates with F-TiO_2, a relative heterojunction photocatalyst TiN/F-TiO_2 is formed, which may improve charge separation and photocatalytic activity of the photocatalyst effectively. To the best of our knowledge, however, the study of the composite photocatalyst TiN/F-TiO_2 has not been reported.

In this study, F-TiO_2 and TiN/F-TiO_2 powders were prepared by ball milling using NH_4F solution as a disperser. The photocatalysts were characterized by X-ray powder diffraction (XRD), scanning electron microscopy (SEM), transmission electron microscopy (TEM), terephthalic acid photoluminescence probing technique (TA-PL), X-ray photoelectron spectroscopy (XPS), and UV–vis diffuse reflection spectroscopy (DRS). The photocatalytic activity of the photocatalysts was evaluated by photocatalytic oxidation of methylene blue (MB) and rhodamine B (RhB). The desired result was obtained. It showed that the photocatalytic activity of the TiN/F-TiO_2 photocatalyst was much higher than that of TiO_2 and the mixture of TiN and F-TiO_2 without ball milling under UV light irradiation. The effect of ball milling time on the photocatalytic activity of the photocatalysts was also investigated. The mechanisms of influence on the photocatalytic activity of the TiN/F-TiO_2 photocatalyst were also discussed.

* Corresponding authors. Tel.: +86 561 3806611; fax: +86 561 3803141.
E-mail address: chshifu@chnu.edu.cn (C. Shifu).

0304-3894/$ – see front matter © 2010 Elsevier B.V. All rights reserved.
doi:10.1016/j.jhazmat.2010.12.046

2. Experimental

2.1. Materials

The TiO_2 powder (Anatase 90%, Rutile 10%, with crystallite size of approximately 50–60 nm) used in the experiments was supplied by Sinopharm Chemical Reagent Co Ltd. TiN powder (99.5%) was supplied by a Johnson Matthey Company. NH_4F was of analytically pure grade, and purchased from Shanghai Chemical Reagent Co Ltd. Methylene blue (MB), rhodamine B and other chemicals used in the experiments were purchased from Shanghai and other China chemical reagent Ltd. They were of analytically pure grade. Deionized water was used throughout this study.

2.2. Preparation of F-TiO_2 and TiN/F-TiO_2

The preparation of F-TiO_2 photocatalyst was carried out in a ND2-2L ball mill (made in Tianzun Electronics Co Ltd., Nanjing University). The procedures for the preparation of F-TiO_2 were as follows: 5.0 g TiO_2 powder and three different size Zirconia balls were mixed in the Zirconia tank, and then a certain amount of NH_4F (0 g, 0.2 g, 0.5 g, 1.0 g, 1.5 g, 2.0 g, 2.5 g) and H_2O (5 mL) were added. After being milled for a certain time (0–24 h) at the speed of 550 rpm, the wet powder was dried at 110 °C in the air. The final samples were used for the determination of photocatalytic activity and characterization. The TiN/F-TiO_2 photocatalyst was prepared in the same procedure. For each sample, 1.0 g NH_4F, 5.0 g TiO_2, and 5.0 mL H_2O were added in a Zirconia tank, varying the weight ratio of TiN(0%, 0.03%, 0.05%, 0.07%, 0.1%, 0.2%, 0.5% and 1%), and then different TiN/F-TiO_2 powder samples were prepared, respectively.

2.3. Photoreaction apparatus and procedure

Experiments were carried out in a photoreaction apparatus [24]. The photoreaction apparatus consists of two parts. The first part is an annular quartz tube. A 375 W medium pressure mercury lamp (Institute of Electric Light Source, Beijing) with a maximum emission at about 365 nm was used as UV light sources. The lamp is laid in the empty chamber of the annular tube, and running water passes through an inner thimble of the annular tube. Owing to continuous cooling, the temperature of the reaction solution is maintained at approximately 30 °C. The second part is an unsealed beaker with a diameter of 12 cm. At the start of the experiment, the reaction solution (volume, 300 mL) containing reactants and photocatalyst was put in the unsealed beakers, and a magnetic stirring device was used to stir the reaction solution. The distance between the light source and the surface of the reaction solution is 11 cm. In the experiments, the initial pH of the reaction solution was 5.0, the illumination time was 10 min, and the amount of the photocatalyst used was 2.0 g/L, the initial concentrations of MB and RhB were 1.0×10^{-4} mol/L and 1.0×10^{-5} mol/L, respectively. In order to disperse the photocatalyst powder, the suspensions were ultrasonically vibrated for 20 min prior to irradiation. After illumination, the samples (volume of each was 5 mL) taken from the reaction suspension were centrifuged at 7000 rpm for 20 min and filtered through a 0.2 μm millipore filter to remove the particles. The filtrate was then analyzed. In order to determine the reproducibility of the results, at least duplicated runs were carried out for each condition for averaging the results, and the experimental error was found to be within ±4%.

2.4. Characterization

In order to determine the crystal phase composition and the crystallite size of the photocatalysts, X-ray diffraction measurement was carried out at room temperature using a DX-2000 X-ray powder diffractometer with Cu Kα radiation and a scanning speed of 3°/min. The accelerating voltage and emission current were 40 kV and 30 mA, respectively. The crystallite size was calculated by X-ray line broadening analysis using the Scherrer equation.

The microcrystalline structure and surface characteristics of the photocatalysts were also investigated by using (X-650 Japan) scanning electron microscopy (SEM).

Transmission electron microscopy and high-resolution transmission electron microscopy (HR-TEM) images were performed with a JEOL-2010 transmission electron microscope, using an accelerating voltage of 200 kV.

UV–vis diffuse reflectance spectroscopy measurements were carried out using a Hitachi UV-365 spectrophotometer equipped with an integrating sphere attachment. The analysis range was from 250 to 650 nm, and $BaSO_4$ was used as a reflectance standard.

X-ray photoelectron spectroscopy was carried out on a Thermo ESCALAB 250 multifunctional spectrometer (VG Scientific UK) using Al Kα radiation. All XPS spectra were referenced to the C1s peak at 284.8 eV from adventitious hydrocarbon contamination.

Photoluminescence emission spectra were recorded on a JASCO FP-6500 type fluorescence spectrophotometer over a wavelength range of 360–500 nm.

2.5. Analysis

The concentration of MB and RhB in solution was determined by spectrophotometer. The photoxidation conversion of MB and RhB was calculated from the following expression:

$$\eta = \frac{C_0 - C_t}{C_0} \times 100$$

where η is the photocatalytic conversion; C_0 is the concentration of reactant before illumination; C_t is the concentration of reactant after illumination time t.

3. Results and discussion

3.1. Effect of the amount of NH_4F on the photocatalytic activity of F-TiO_2

The blank test shows that photo-induced self-sensitized photodegradation has little influence on the photocatalytic oxidation of MB and RhB. The fixed ball milling time and illumination time for each sample is 12 h and 10 min, respectively. Fig. 1 shows the

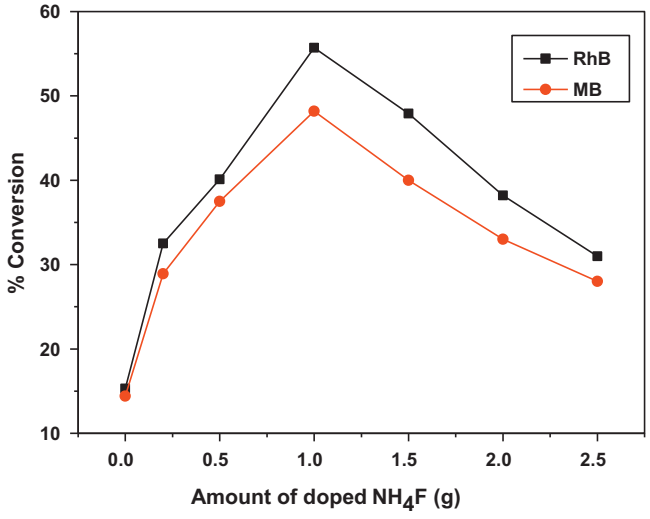

Fig. 1. Effect of the amount of NH_4F on the photocatalytic activity of F-TiO_2.

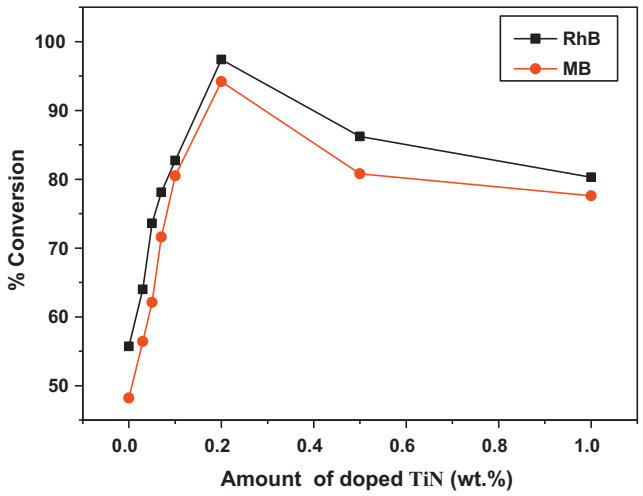

Fig. 2. Effect of the amount of doped TiN on the photocatalytic activity of TiN/F-TiO_2.

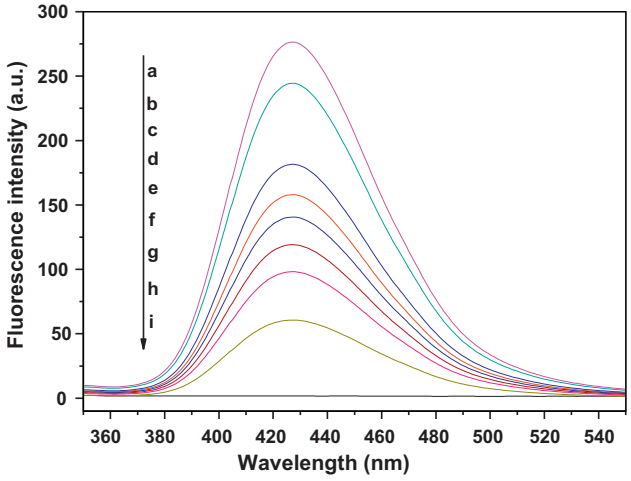

Fig. 3. Changes of PL spectra of different samples: (a) TiN(0.2 wt.%)/F-TiO_2, (b) TiN(0.5 wt.%)/F-TiO_2, (c) TiN(0.03 wt.%)/F-TiO_2, (d) F-TiO_2(NHF_4:1.0 g), (e) F-TiO_2(NHF_4:1.5 g), (f) F-TiO_2(NHF_4:2.0 g), (g) F-TiO_2(NHF_4: 0.2 g), (h) TiO_2, (i) pure terephthalic acid.

effect of the amount of NH_4F on the photocatalytic activity of the photocatalysts.

From Fig. 1, it can be seen that, if NH_4F is absent, namely, with the pure TiO_2 powder photocatalyst, its photooxidation activity is the lowest, and the photooxidation conversion for MB and RhB is 14.4% and 15.3%, respectively. The photooxidation activity of F-TiO_2 increases remarkably with the increase of the amount of NH_4F up to 1.0 g. When the amount of NH_4F is 1.0 g, the photocatalytic activity of the F-TiO_2 photocatalyst is at its peak, and the photooxidation conversion of MB and RhB is 48.2% and 55.7%, respectively. When the amount of NH_4F is higher than the optimal amount, the photooxidation activity of F-TiO_2 decreases gradually.

3.2. Effect of the amount of doped TiN on the photocatalytic activity of TiN/F-TiO_2

The fixed ball milling time for each sample was 12 h. The amount of TiO_2 and NH_4F was 5.0 g and 1.0 g, respectively. Fig. 2 shows the effects of amount of doped TiN on the photocatalytic activity of TiN/F-TiO_2.

The fixed illumination time for each experiment was 10 min. From Fig. 2, it can be seen that the photocatalytic activity of TiN/F-TiO_2 increases remarkably with the increase of the amount of doped TiN up to 0.2%. The optimum amount of doped TiN is 0.2%, and the photodegradation conversion for RhB and MB is 97.4% and 94.2%, respectively. When the amount of doped TiN is higher than the optimal amount, the photocatalytic activity of TiN/F-TiO_2 decreases gradually. The results also show that if TiN is absent, namely, the pure F-TiO_2 powder photocatalyst, its photooxidation conversion for MB and RhB is 48.2% and 55.7%, respectively. It is clear that the photocatalytic activity of TiN/F-TiO_2 is higher than that of F-TiO_2 photocatalyst. It is known that, TiN can be dissociated to Ti^{3+} in the ball milling process, and the amount of Ti^{3+} increases greatly after a suitable amount of TiN loading on TiO_2 by ball milling. Ti^{3+} on the surface of TiO_2 is the most reactive center for the photocatalytic process, which may be a surface defect and offers unique site for oxygen chemical adsorption, and results in the high activity of the corresponding photocatalyst [24,25]. Another important reason may be that the F-TiO_2 doped with the suitable amount of TiN, the coupled photocatalyst can be formed between TiN and F-TiO_2 by the ball milling method, which prolongs the lifetime of the carriers and improves the photocatalytic activity. However, after adding redundant TiN, Ti^{3+} ions can enter into the photocatalyst lattice in the process of ball milling and the inner Ti^{3+} may become a recombination center of carriers, so the photocatalytic activity decreases steadily.

3.3. Hydroxyl radical analysis

The formation of hydroxyl radicals (•OH) on the surface of F-TiO_2 and TiN/F-TiO_2 photocatalyst is detected by a photoluminescence (PL) technique with terephthalic acid as a probe molecule. The method is rapid, sensitive, and specific, which only needs simple standard PL instrumentation. Terephthalic acid reacts with •OH readily to produce a highly fluorescent product, 2-hydroxyterephthalic acid, whose PL peak intensity is in proportion to the amount of OH radicals produced in water. Experimental procedures were reported in earlier reports [23]. After UV irradiation for 15 min, the reaction solution was filtrated to measure the increase of the PL intensity at 425 nm excited by 315 nm light of 2-hydroxyterephthalic acid.

Fig. 3 shows the changes of PL spectra of different samples from 5×10^{-4} mol/L terephthalic acid solution in 2×10^{-3} mol/L NaOH with irradiation. From Fig. 3, it can be seen that, the PL peak of TiN(0.2 wt.%)/F-TiO_2 is higher than any other samples, and it suggests that the formation rate of OH radicals on its surface is much higher than that of the other powders. When the amount of TiN is too small or redundant, the surface of TiN/F-TiO_2 sample inhibits the production of OH radicals, which implies the photocatalytic oxidation activity of the photocatalyst is much lower than that of TiN(0.2 wt.%)/F-TiO_2. Similarly, when the amount of NH_4F is lower or higher than 1.0 g, the production of OH radicals is inhibited and the photocatalytic oxidation activity of the F-TiO_2 photocatalyst decreases. The same results are verified in the Sections 3.1 and 3.2.

3.4. Effect of the ball milling time on the photocatalytic activity of F-TiO_2 and TiN/F-TiO_2

The fixed amount of NH_4F was 1.0 g. The amount of TiN in the sample was 0.2 wt.%, and the illumination time for each sample was 10 min. The relationship between the photocatalytic activity and the ball milling time varying from 0 to 36 h was investigated. The result is shown in Fig. 4.

From Fig. 4, it is clear that the ball milling time influences the photocatalytic activity greatly under UV light irradiation. It is obvious that the photocatalytic activity of the F-TiO_2 and TiN/F-TiO_2 is much higher than that of the mixture of NH_4F-TiO_2 and TiN-NH_4F-

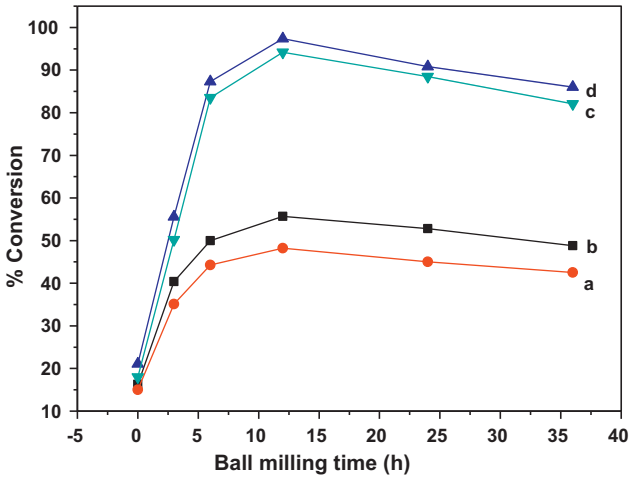

Fig. 4. Effect of the ball milling time on the photocatalytic activity: (a) MB (F-TiO_2), (b) RhB (F-TiO_2), (c) MB (TiN/F-TiO_2), (d) RhB (TiN/F-TiO_2).

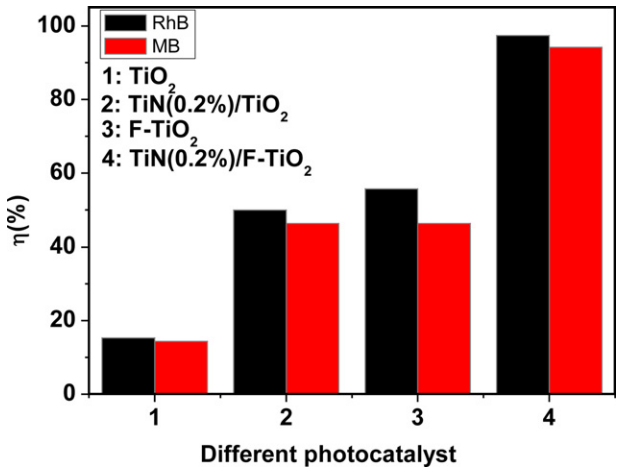

Fig. 5. Photocatalytic activity of TiO_2, TiN(0.2%)/TiO_2, F-TiO_2 and TiN(0.2%)/F-TiO_2.

TiO_2 without ball milling. The photocatalytic conversions of four different samples have similar trend lines. The photocatalytic conversions increase rapidly with the increase of the ball milling time up to 12 h. When the ball milling time is longer than 12 h, the photocatalytic conversions decrease gradually. Without ball milling, the photocatalytic activities of the samples are the lowest, and the conversions of a, b, c and d are 15.0%, 16.3%, 18.0%, and 21.1%, respectively. When the ball milling time is 12 h, the photocatalytic activities of the samples reach their maximum and the conversions of a, b, c and d are 48.2%, 55.7%, 94.2%, and 97.4%, respectively.

F-TiO_2 enhanced the photodegradation of RhB and MB in aqueous solutions. It was proposed that the fluorinated surface favored the generation of free OH radicals, which was responsible for the enhanced photocatalytic oxidation activity [23]. The possible reason for the increased photocatalytic activity of the photocatalyst TiN/F-TiO_2 may be attributed to the fact that TiO_2 and TiN only play their own photocatalytic role without ball milling, and the heterojunction photocatalyst is not formed. However, TiO_2 and TiN can form heterojunction photocatalyst after ball milling. The heterojunction photocatalyst TiN/F-TiO_2 conduces to the separation of the photoexcited electron–hole pairs effectively, and the photocatalytic activity is enhanced. When the ball milling time is lower than 12 h, with the ball milling time increasing, the F ions on the photocatalyst surface may enter into the photocatalyst lattice so that the absorption wavelength red shifts and the photocatalytic activity is improved remarkably. Meanwhile, the amount of Ti^{3+} on the surface of the photocatalyst increases, which is the most reactive center for the photocatalytic process [26]. At the same time, with the increase of the ball milling time, the specific surface area of the photocatalyst increases [20]. Correspondingly, the number of active sites per unit weight of the photocatalyst also increases. However, when the ball milling time is longer than the optimal time, it is proposed that with the increase of the ball milling time, the fresh surface formed by high-energy ball milling possesses high surface energy and prefers to agglomerate. The assumption is proved by the results of SEM. At the same time, a number of crystal defects and inner Ti^{3+} in the TiO_2 lattice are produced during high-energy ball milling. And the crystal defects and the inner Ti^{3+} will become recombination centers of the photogenerated electrons and holes.

3.5. Comparison of photocatalytic activity among the TiO_2, TiN(0.2%)/TiO_2, F-TiO_2 and TiN(0.2%)/F-TiO_2

The fixed ball milling time for each sample was 12 h. The amount of TiO_2 and NH_4F was 5.0 g and 1.0 g, respectively. The photocatalytic activity of the samples was investigated by photocatalytic oxidation of rhodamine B and MB. All of the data obtained are corrected for absorption after stirring for 20 min in the dark.

Fig. 5 shows the photodegradation of RhB and MB over pure TiO_2, TiN(0.2%)/TiO_2, F-TiO_2, and TiN(0.2%)/F-TiO_2 under UV light radiation. It can be seen that the photocatalytic activity of heterostructure TiN/F-TiO_2 is the highest, and the photocatalytic activity of TiN/TiO_2 and F-TiO_2 is higher than that of pure TiO_2. At the same time, it is clear that the photocatalytic activity of F-TiO_2 is a little higher than that of TiN/TiO_2.

3.6. Characterization of the F-TiO_2 and TiN/F-TiO_2 photocatalysts

3.6.1. XRD analysis

The fixed ball milling time is 12 h. The XRD patterns of different photocatalysts are shown in Fig. 6. It is clear that when the amount of doped TiN is less than 5.0 wt.%, the diffraction peaks of TiN cannot be found in XRD patterns. This illustrates that TiN is highly dispersed in the bulk phase of the catalyst. When the amount of doped TiN is higher than 5.0 wt.%, the diffraction peaks of TiN can be found in XRD patterns. Since no new crystal phases are found, it can be concluded that there are no new materials formed in the ball milling process, or the new crystal phases formed in the process of

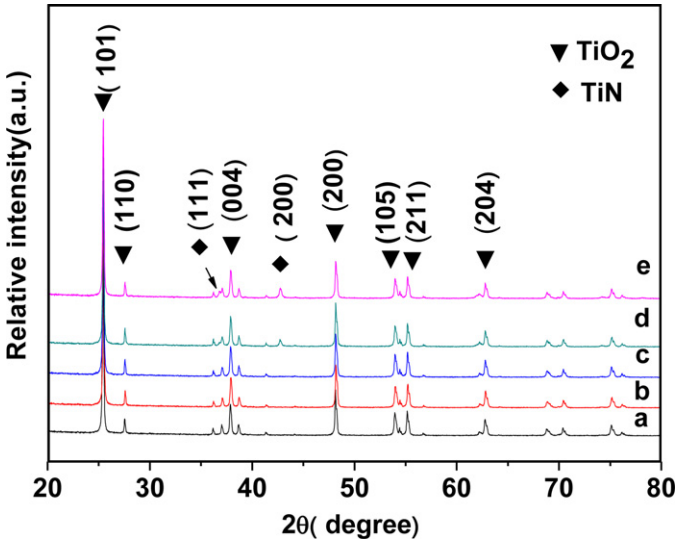

Fig. 6. XRD patterns of different photocatalysts: (a) F-TiO_2, (b) TiN(0.05 wt.%)/F-TiO_2, (c) TiN(0.1 wt.%)/F-TiO_2, (d) TiN(5.0 wt.%)/F-TiO_2 (e) TiN(10.0 wt.%)/F-TiO_2.

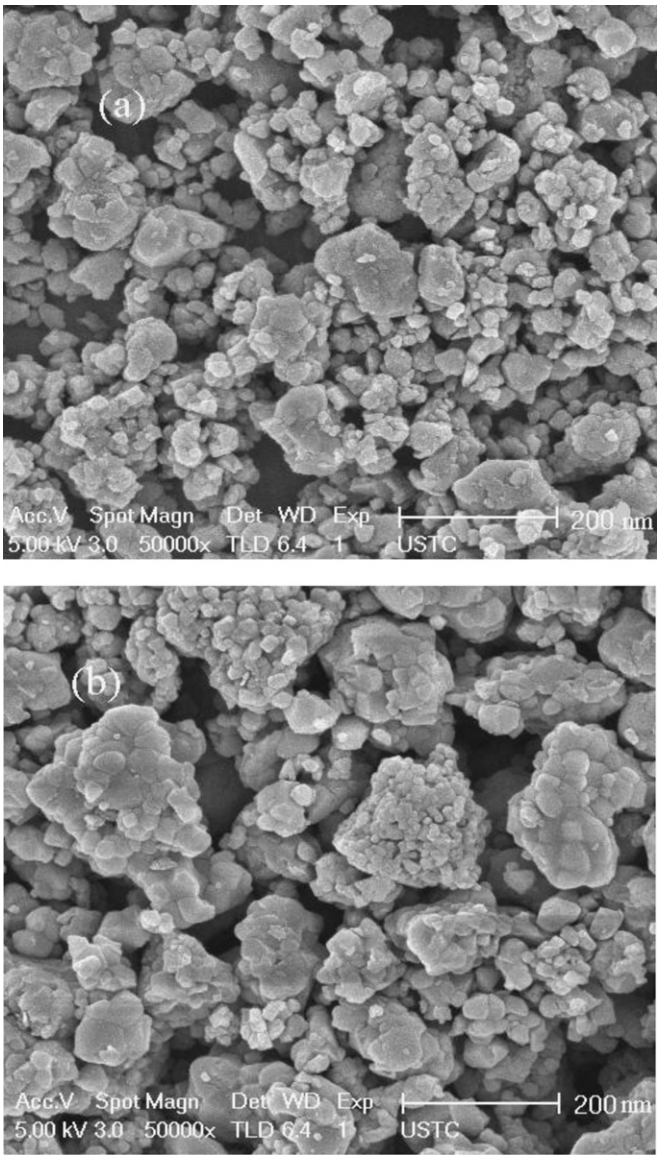

Fig. 7. SEM images of TiN(0.2 wt.%)/F-TiO_2 photocatalysts: (a) TiN(0.2 wt.%)/F-TiO_2, ball milling time 12 h, (b) TiN(0.2 wt.%)/F-TiO_2, ball milling time 24 h.

ball milling are so small that they cannot be detected in the experimental condition. The similar result was reported in Ref [27]. It is known by the calculation from the Scherrer equation that the diameter of the photocatalyst is not obviously changed. The crystallite size is about 50 nm.

3.6.2. SEM analysis

SEM was used to investigate the morphology of the samples. Fig. 7 shows SEM images of TiN(0.2 wt.%)/F-TiO_2 photocatalysts. It can be seen that the appearance is shapeless sheet, and the average diameter of the photocatalyst is about 45–55 nm. The result is the same as that of XRD. From Fig. 7, it also can be seen that when the ball milling time is 12 h, the dispersion degree of the sample is higher than that of the sample ball milled for 24 h. Namely, when the ball milling time is longer than the optimum time, the fresh surfaces formed by high-energy ball milling possess high surface energy and prefers to agglomerate with the increase of the ball milling time. The similar result was reported in Ref. [27].

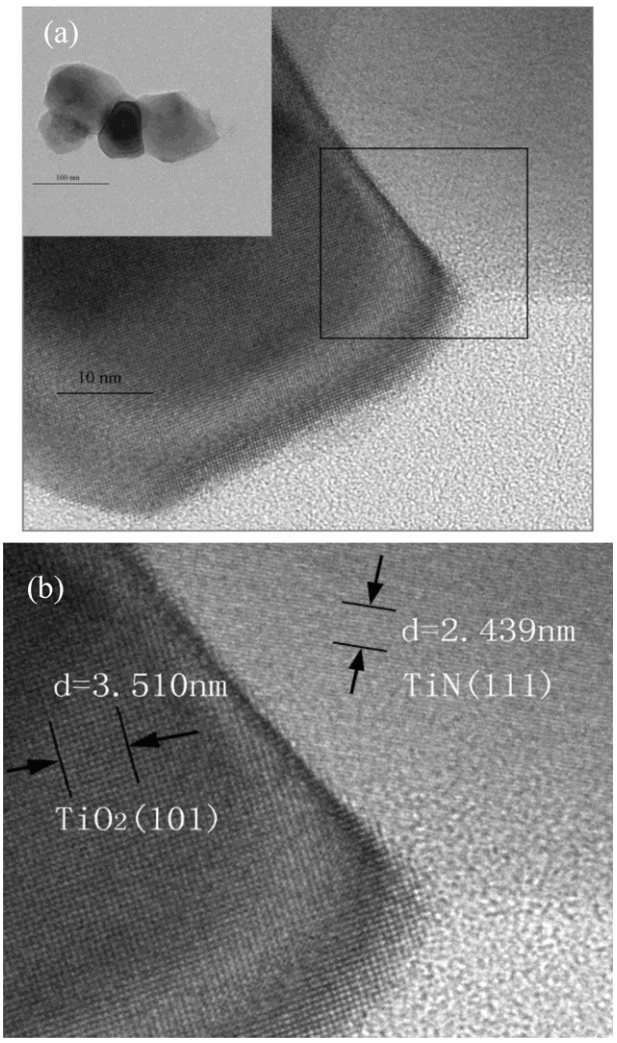

Fig. 8. TEM and HR-TEM images of TiN(0.2 wt.%)/F-TiO_2 photocatalys: (a) TEM image, (b) HR-TEM image.

3.6.3. TEM analysis

In order to investigate the interface of the sample, the TiN(0.2 wt.%)/F-TiO_2 photocatalyst was chosen for TEM and high resolution TEM (HR-TEM) characterization.

Fig. 8a gives an overview of the typical TEM image of the heterojunction TiN(0.2 wt.%)/F-TiO_2 photocatalyst. It clearly exhibits the existence of TiN nanoparticles with mean sizes of about 60–70 nm dispersing over the particle of TiO_2. Fig. 8b shows the HR-TEM image of the sample corresponding to the rectangle region of the TEM image in Fig. 8a. The upper part depicts the (1 1 1) plane of TiN with a spacing of 2.439 nm. The lower part depicts the (1 0 1) plane of TiO_2 with a spacing value of 3.510 nm. The good crystalline quality and the clear interface between TiN and TiO_2 are advantageous for the separation of the photogenerated charge carriers. Based on the above results, it is suggested that the heterojunction will be formed by ball milling between TiN and TiO_2.

3.6.4. UV–vis analysis

Fig. 9 shows UV–vis diffuse reflectance spectra of F-TiO_2 and a series of TiN/F-TiO_2 photocatalysts. The samples were ball milled for 12 h, respectively. It is known that the band gap of TiO_2 is about 3.2 eV and it can be excited by photons with wavelengths below 387 nm. Fig. 9 shows that compared with pure TiO_2, the absorption wavelength range of the F-TiO_2 is extended greatly towards visible light with the F^- doped. And it will increase the number of photo-

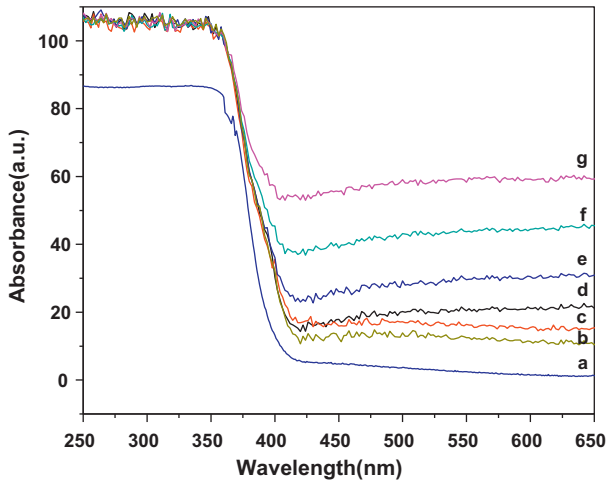

Fig. 9. UV–vis diffuse reflectance spectra of different photocatalysts: (a) TiO_2, (b) F-TiO_2, (c) TiN(0.03 wt.%)/F-TiO_2, (d) TiN(0.05 wt.%)/F-TiO_2, (e) TiN(0.07 wt.%)/F-TiO_2, (f) TiN(0.1 wt.%)/F-TiO_2, (g) TiN(0.2 wt.%)/F-TiO_2.

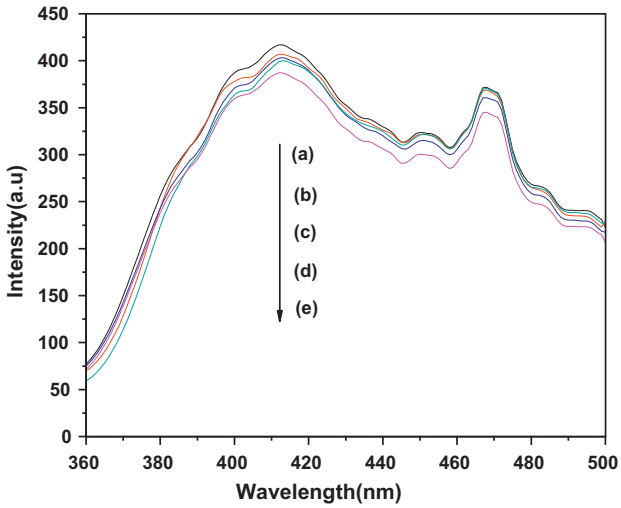

Fig. 10. Photoluminescence emission spectra of pure TiO_2 and different F-TiO_2 photocatalysts: (a) TiO_2, (b) NH_4F (0.20 g)-TiO_2, (c) NH_4F (0.50 g)-TiO_2, (d) NH_4F (1.50 g)-TiO_2, (e) NH_4F (1.0 g)-TiO_2.

generated electrons and holes to participate in the photocatalytic reaction, which will enhance the photocatalytic activity of F-TiO_2 powders [28]. For F-TiO_2, the presence of a strong absorption band at a low wavelength in the spectra near 350 nm indicates that the Ti species are tetrahedral Ti^{4+}. This absorption band is generally associated with the electronic excitation of the valence band O2p electron to the conduction band Ti3d level [19,29]. Compared with F-TiO_2, the absorption edge extends a little to longer wavelength for the photocatalyst TiN/F-TiO_2, revealing the good contact between TiN and F-TiO_2 crystallites as a consequence of the inter-dispersion of the two phases, which is produced by ball milling process. The photoexcited wavelength range of the photocatalyst is connected with the amount of TiN. It increases with the increase of the amount of TiN. The extension of absorption wavelength range can probably be attributed to the introduction of Ti^{3+} and the formation of a defective energy level in the particles during the ball milling process. Because the absorption wavelength range is extended greatly towards visible light and the absorption intensity increases, the formation rate of electron–hole pairs on the photocatalyst surface also increases greatly, which results in the photocatalyst exhibiting higher photocatalytic activity. The results are consistent with the evaluation of photocatalytic activity. There were similar results in previous report [30].

3.6.5. *Photoluminescence emission spectra*

The Photoluminescence emission spectra have been widely used to investigate the efficiency of charge carrier trapping, immigration and transfer, and to understand the fate of electron–hole pairs in semiconductor particles for photoluminescence emission is resulted from the recombination of free carriers [31,32]. In this study, an ultraviolet light with a 260 nm wavelength as the excitation source was used for get the fluorescence emission spectra of the different samples. The results are shown in Figs. 10 and 11, respectively. It can be seen that the pure TiO_2 samples have a stronger emission peak at around 410 nm and a weaker emission peak at around 470 nm, showing indirect band gap characteristics [33].

From Fig. 10, it is clear that the relative intensity of the emission spectra of TiO_2 has the greatest relative intensity, which means that electrons and holes of TiO_2 are easy to recombine. The relative intensity of the F-TiO_2 photocatalyst is lower than that of TiO_2, showing that the doped NH_4F is helpful to inhibit the recombination of electrons and holes and to improve the photocatalytic activity. The amount of NH_4F can influence the thickness of the superficial space-charge layer of TiO_2. When the amount of NH_4F is 1.0 g, the relative intensity of emission spectra is the lowest, which shows that 1.0 g doping quantity of NH_4F can effectively restrain the recombination of electrons and holes. When the NH_4F content is too small, the recombination rate of electron–hole pairs is high due to the absence of adequate traps. When the doping quantity is considerably high, the absorption of light and the generation of electrons–holes are both decreased.

From Fig. 11, it can be seen that the photoluminescence spectra are quite sensitive to the doping amount of TiN. Due to doping TiN, the photoluminescence emission intensity of the different TiN/F-TiO_2 photocatalysts is lower than that of F-TiO_2. When the amount of doped TiN varies from 0% to 0.2 wt.%, the photoluminescence emission intensity decreases accordingly. However, if the amount of TiN is 0.5 wt.%, the photoluminescence emission intensity is higher than that of the 0.2 wt.% TiN. The result is consistent with that of the photocatalytic activity experiment.

It is known that the photoluminescence emission intensity is the result of the recombination of photoexcited electrons and holes, and the lower photoluminescence emission intensity indicates a

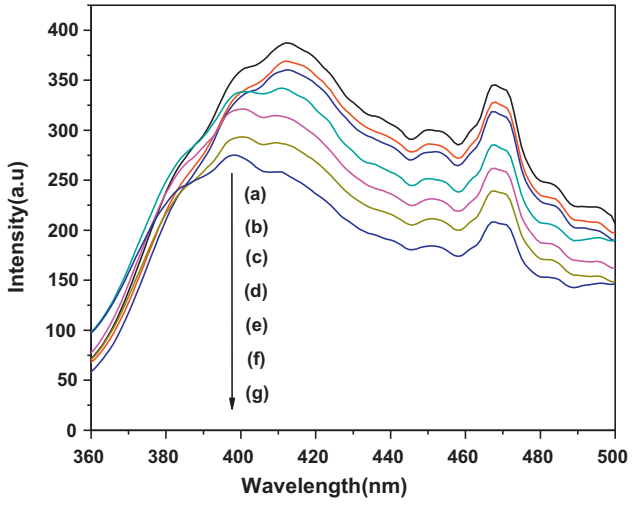

Fig. 11. Photoluminescence emission spectra of pure TiN and different TiN/F-TiO_2 photocatalysts: (a) F-TiO_2, (b) TiN(0.03 wt.%)/F-TiO_2, (c) TiN(0.05 wt.%)/F-TiO_2, (d) TiN(0.07 wt.%)/F-TiO_2 (e) TiN(0.1 wt.%)/F-TiO_2, (f) TiN(0.5 wt.%)/F-TiO_2, (g) TiN(0.2 wt.%)/F-TiO_2.

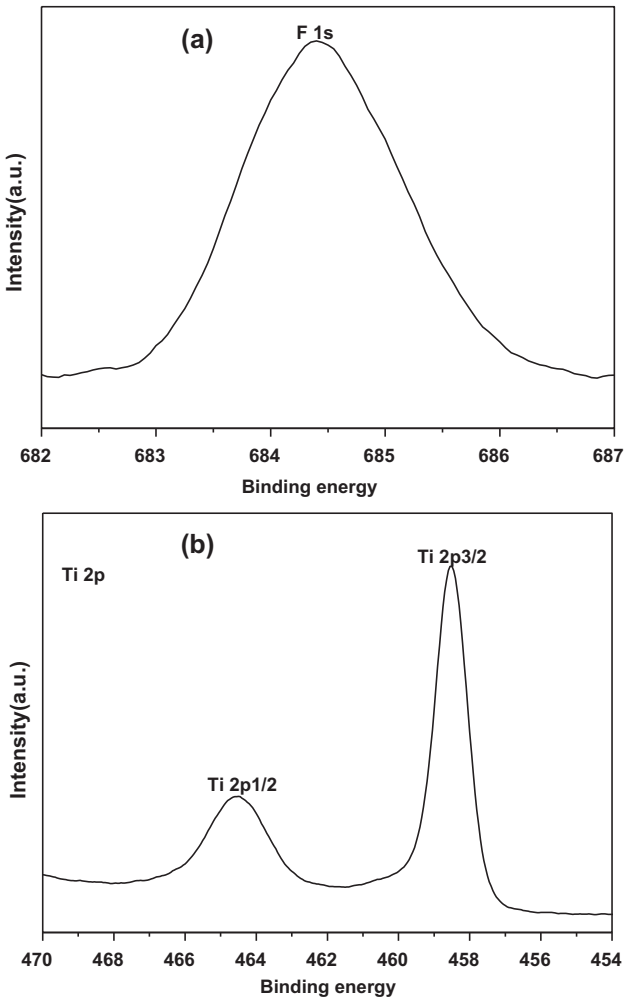

Fig. 12. High resolution scanning XPS spectra.

lower recombination rate of photoexcited electron–hole [34]. Consequently, compared with pure TiO_2, doping NH_4F and TiN into samples will enhance the charge separation efficiency of the photoexcited electrons and holes. That is to say that doping proper NH_4F and TiN is helpful to inhibit the recombination of electrons and holes, which improves the photocatalytic activity.

3.6.6. XPS analysis

To identify the chemical state of F and Ti atoms in the photocatalyst, the X-ray photoelectron spectroscopy (XPS) of the TiN(0.2%)/F-TiO_2 ball milled for 12 h was measured. The result is shown in Fig. 12. From the high resolution scanning XPS spectra of F 1s (Fig. 12a), it can be seen that the photoelectron peaks for F 1s appear clearly at the binding energy of 684 eV, which is due to the surface fluoride of TiO_2. The surface fluoride (≡TiO_2-F) was formed by the ligand exchange reaction between F^- and the surface hydroxyl group on the surface of TiO_2. From Fig. 12b, the oxidation and spin state of the atoms match well with standard Ti 2p1/2 and Ti 2p3/2 peaks, indicating that the two peaks are approximately consistent with the data of Ti2p provided by the databank [35,36]. However, there are no signal of F ion in the lattice (BE = 688.5 eV) of the sample and peak shoulder at 456.7 eV attributed to Ti^{3+} in the high resolution scanning spectra [23,24]. It may be attributed to the fact that the contents of F ion and Ti^{3+} are so small that they cannot be detected in the experimental condition.

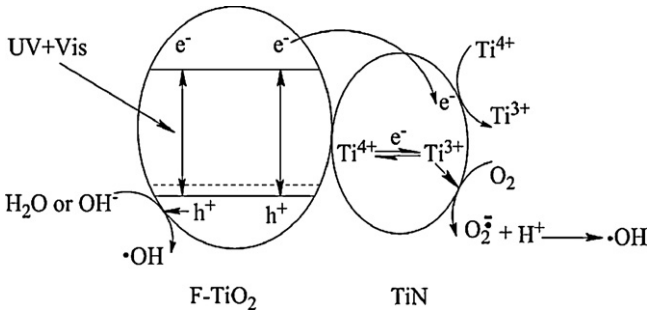

Fig. 13. Schematic diagram of charge separation and the photocatalytic activity for the photocatalyst.

3.7. Discussion of mechanism

It is known that surface fluorination can be done by a simple ligand exchange between surface hydroxyl groups on TiO_2 and fluoride ions [34].

$$\equiv Ti{-}OH + F^- \leftrightarrow \equiv Ti{-}F + OH^-$$

Minero et al. confirmed that fluoride enhanced the photodecomposition of phenol with TiO_2 in aqueous solutions and proposed that the fluorinated surface favored the generation of free OH radicals, which was responsible for the enhanced photocatalytic oxidation activity [23,37]. Meanwhile, with the increase in the ball milling time, the F ions on the photocatalyst surface may enter into the photocatalyst lattice, which results in the absorption wavelength red shifts, and the photocatalytic activity is increased. At the same time, Ti^{3+} on the TiO_2 surface is produced during high-energy ball milling. Surface Ti^{3+} is the most reactive center for photocatalytic process, and the Ti^{3+} on the surface of TiO_2 is the unique site for oxygen chemical adsorption. $O_2^{\bullet -}$ may be produced by the reaction of Ti^{3+} and O_2, so the photocatalytic activity is improved. Furthermore, it is proposed that when TiN integrates with the F-TiO_2 granule, a number of micro heterojunction photocatalyst TiN/F-TiO_2 are formed. At the equilibrium, the inner electric field is formed in the junction between TiN and TiO_2. Under near UV illumination, the photogenerated electron–hole pairs will be separated effectively by the heterojunction formed in the TiN/F-TiO_2. Therefore, the photocatalytic activity of the TiN/F-TiO_2 photocatalyst is enhanced greatly. The schematic diagram of charge separation and the photocatalytic activity for the photocatalysts is shown in Fig. 13.

4. Conclusions

The F-TiO_2 and TiN/F-TiO_2 nanoparticle photocatalyst were prepared by ball milling. The photocatalytic activity of the TiN/F-TiO_2 is much higher than that of TiO_2, F-TiO_2, and the mixture of TiN/F-TiO_2 without ball milling. The optimum percentage of doped TiN is 0.2 wt.%. The ball milling time has a significant influence on the photocatalytic activity of the photocatalyst. The optimum ball milling time is 12 h. Compared with pure TiO_2, the photoabsorption wavelength range of the F-TiO_2 and TiN/F-TiO_2 photocatalysts red shifts and improves the utilization of the total spectrum. The increase of the Ti^{3+} reactive center on the surface and the extension of the photoabsorption wavelength are favorable for the increase of the photocatalytic activity of the TiN/F-TiO_2. Another important reason may be attributed to the formation of the heterojunction between TiN and F-TiO_2, the photogenerated electrons and holes are separated efficiently, and the photocatalytic activity of the photocatalyst is enhanced greatly.

Acknowledgements

This study was supported by the Natural Science Foundation of China (no. 20673042, 20973071) and the Key Project of Science and Technology Research of the Ministry of Education of China (208062).

References

[1] A. Fujishima, K. Honda, Electrochemical photolysis of water at a semiconductor electrode, Nature 238 (1972) 37–38.
[2] R. Shi, G.L. Huang, J.Y. Lin, F. Zhu, Photocatalytic activity enhancement for Bi_2WO_6 by fluorine substitution, J. Phys. Chem. C 113 (2009) 19633–19638.
[3] D. Zhao, C.C. Chen, C.L. Yu, W.H. Ma, J.C. Zhao, Photoinduced electron storage in WO_3/TiO_2 nanohybrid material in the presence of oxygen and postirradiated reduction of heavy metalions, J. Phys. Chem. C 113 (2009) 13160–13165.
[4] T.J.L. Yan, N. Long, X.C. Shi, D.H. Wang, Z.H. Li, X.X. Wang, Efficient photocatalytic degradation of volatile organic compounds by porous indium hydroxide nanocrystals, Environ. Sci. Technol. 244 (2010) 1380–1385.
[5] J.G. Yu, L.J. Zhang, B. Cheng, Y.R. Su, Hydrothermal preparation and photocatalytic activity of hierarchically sponge-like macro-mesoporous titania, J. Phys. Chem. C 111 (2007) 10582–10589.
[6] C. Hu, Y. Lan, J. Qu, X. Hu, A. Wang, $Ag/AgBr/TiO_2$ visible light photocatalyst for destruction of azodyes and bacteria, J. Phys. Chem. B 110 (2006) 4066–4072.
[7] J.G. Yu, W. Liu, H.G. Yu, A one-pot approach to hierarchically nanoporous titania hollow microspheres with high photocatalytic activity, Cryst. Growth Des. 8 (2008) 930–934.
[8] Y.H. Zheng, C.Q. Chen, Y.Y. Zhan, X.Y. Lin, Q. Zheng, K. Wei, J.F. Zhu, Photocatalytic activity of Ag/ZnO heterostructure nanocatalyst: correlation between structure and property, J. Phys. Chem. C 112 (2008) 10773–10777.
[9] H. Tang, J.C. Chang, Y.Y. Shan, S.T. Lee, Surfactant-assisted alignment of ZnO nanocrystals to superstructures, J. Phys. Chem. B 112 (2008) 4016–4021.
[10] Z.H. Wen, G. Wang, W. Lu, Q. Wang, Q. Zhang, J.H. Li, Enhanced photocatalytic properties of mesoporous SnO_2 induced by low concentration ZnO doping, Cryst. Growth Des. 7 (2007) 1722–1725.
[11] R.Y. Hong, S.Z. Zhang, G.Q. Di, H.Z. Li, Y. Zheng, J. Ding, D.G. Wei, Preparation, characterization and application of Fe_3O_4/ZnO core/shell magnetic nanoparticles, Mater. Res. Bull. 43 (2008) 2457–2468.
[12] C.K.S.J. Doh, S.G. Lee, S.J. Lee, H.Y. Kim, Visible-light absorptivity of a zincoxysulfide (ZnO_xS_{1-x}) composite semiconductor and its photocatalytic activities for degradation of organic pollutants under visible-light irradiation, Appl. Catal. A 330 (2007) 127–133.
[13] X. Wang, P. Hu, Y.F. Li, L.J. Yu, reparation and characterization of ZnO hollow spheres and ZnO-Carbon composite materials using colloidal carbon spheres as templates, J. Phys. Chem. C 111 (2007) 6706–6712.
[14] S. Moribe, T. Ikoma, K. Akiyama, Q.W. Zhang, F. Saito, S.T. Kubota, EPR study on paramagnetic species in nitrogen-doped ZnO powders prepared by a mechanochemical method, Chem. Phys. Lett. 436 (2007) 4–6.
[15] J. Lin, J. Lin, Y.F. Zhu, Controlled synthesis of the $ZnWO_4$ nanostructure and effects on the photocatalytic performance, Inorg. Chem. 46 (2007) 8372–8378.
[16] B. Doggett, S. Chakrabarti, R. O'Haire, A. Meaney, E. McGlynn, M.O. Henry, J.P. Mosnier, Electrical characterisation of phosphorus-doped ZnO thin films grown by pulsed laser deposition, Superlattices Microstruct. 42 (2007) 74–78.
[17] H.J. Liu, R. Yang, S.M. Li, Preparation and characterization of the TiO_2–V_2O_5 photocatalyst with visible-light activity, Rare Met. 25 (2006) 636–642.
[18] H. Lin-Rui, Y. Chang-Zhou, P. Yang, Synthesis and photocatalytic property of SnO_2/TiO_2 nanotubes composites, J. Hazard. Mater. B 139 (2007) 310–315.
[19] W. Liu, S.F. Chen, S.J. Zhang, W. Zhao, H.Y. Zhang, X.L. Yu, Preparation and characterization of p–n heterojunction photocatalyst p-$CuBi_2O_4$/n-TiO_2 with high photocatalytic activity under visible and UV light irradiation, J. Nanopart. Res. 12 (2010) 1355–1366.
[20] S.F. Chen, W. Zhao, W. Liu, S.J. Zhang, Preparation, characterization and activity evaluation of p–n junction photocatalyst p-ZnO/n-TiO_2, Appl. Surf. Sci. 255 (2008) 2478–2484.
[21] H. Park, W. Choi, Effects of TiO_2 surface fluorination on photocatalytic reactions and photoelectrochemical behaviors, J. Phys. Chem. B 108 (2004) 4086–4093.
[22] Y.W. Choi, Pure and modified TiO2 photocatalysts and their environmental applications, Catal. Surv. Asia 10 (2006) 16–28.
[23] J.G. Yu, W.G. Wang, B. Cheng, B.L. Su, Enhancement of photocatalytic activity of mesporous TiO_2 powders by hydrothermal surface fluorination treatment, J. Phys. Chem. C 113 (2009) 6743–6750.
[24] S.F. Chen, S.J. Zhang, W. Zhao, W. Liu, Study on the photocatalytic activity of TiN/TiO_2 nanoparticle formed by ball milling, J. Nanopart. Res. 11 (2009) 931–938.
[25] S.X. Liu, Z.P. Qu, X.W. Han, C.L. Sun, A mechanism for enhanced photocatalytic activity of silver-loaded titanium dioxide, Catal. Today 93 (2004) 877–884.
[26] S.X. Liu, Removal of copper (VI) from aqueous solution by Ag/TiO_2 photocatalysis, Bull. Environ. Contam. Toxicol. 74 (2005) 706–714.
[27] S.F. Chen, L. Chen, S. Gao, G.Y. Cao, The preparation of nitrogen-doped photocatalyst $TiO_{2-x}N_x$ by ball milling, Chem. Phys. Lett. 413 (2005) 404–409.
[28] J.C. Yu, J.G. Yu, W.K. Ho, Z.T. Jiang, L.Z. Zhang, Effects of F-doping on the photocatalytic activity and microstructures of nanocrystalline TiO_2 powders, Chem. Mater. 14 (2002) 3808–3816.
[29] A. Fuerte, M.D. Hernández-Alonso, A.J. Maira, A. Martıĭnez-Arias, J. Soria, J.C. Conesa, G. Munuera, M. Fernández-Garcıĭa, Nanosize Ti–W mixed oxides: Effect of doping level in the photocatalytic degradation of toluene using sunlight-type excitation, J. Catal. 212 (2002) 1–9.
[30] S.F. Chen, S.J. Zhang, W. Liu, W. Zhao, Preparation and activity evaluation of p–n junction photocatalyst NiO/TiO_2, J. Hazard. Mater. 155 (2008) 320–326.
[31] T.J. Cai, M. Yue, X.W. Wang, Q. Deng, Preparation, characterization, and photocatalytic performance of $NdPW_{12}O_{40}/TiO_2$ composite catalyst, Chin. J. Catal. 28 (2007) 10–16.
[32] J.W. Tang, Z.G. Zou, J.H. Ye, Photophysical and photocatalytic properties of $AgInW_2O_8$, J. Phys. Chem. B 107 (2003) 14265–14269.
[33] Y. Cong, J. Zhang, F. Chen, M. Anpo, Synthesis and characterization of nitrogen-doped TiO_2 nanophotocatalyst with high visible light activity, J. Phys. Chem. C 111 (2007) 6976–6982.
[34] G. Hopfengärtner, D. Borgmann, I. Rademacher, G. Wedler, E. Hums, G.W. Spitznagel, XPS studies of oxidic model catalysts: internal standards and oxidation numbers, J. Electron Spectrosc. 63 (1993) 91–116.
[35] J.G. Yu, S.W. Liu, S. Mann, Synergetic codoping in fluorinated Ti1-*x*ZrxO2 hollow microspheres, J. Phys. Chem. C 113 (2009) 10712–10717.
[36] J.G. Yu, M.H. Zhou, B. Cheng, X.J. Zhao, Preparation, characterization and photocatalytic activity of in situ N S-codoped TiO_2 powders, J. Mol. Catal. A 246 (2006) 176–184.